Materials Research Letters

ISSN: 2166-3831 (Online) Journal homepage: www.tandfonline.com/journals/tmrl20

Columnar grain boundaries are the weakest link in hard coatings: insights from micro-cantilever testing

Yinxia Zhang, Matthias Bartosik, Steffen Brinckmann, Ujjval Bansal, Subin Lee & Christoph Kirchlechner

To cite this article: Yinxia Zhang, Matthias Bartosik, Steffen Brinckmann, Ujjval Bansal, Subin Lee & Christoph Kirchlechner (2025) Columnar grain boundaries are the weakest link in hard coatings: insights from micro-cantilever testing, Materials Research Letters, 13:11, 1099-1107, DOI: 10.1080/21663831.2025.2560526

To link to this article: https://doi.org/10.1080/21663831.2025.2560526

MATER. RES. LETT.
2025, VOL. 13, NO. 11, 1099–1107
https://doi.org/10.1080/21663831.2025.2560526

MATERIALS RESEARCH LETTERS
Taylor & Francis
Taylor & Francis Group

ORIGINAL REPORT

Columnar grain boundaries are the weakest link in hard coatings: insights from micro-cantilever testing

Yinxia Zhang[a], Matthias Bartosik[b], Steffen Brinckmann[c], Ujjval Bansal[a], Subin Lee[a] and Christoph Kirchlechner[a]

[a]Institute for Applied Materials, Karlsruhe Institute of Technology, Karlsruhe, Germany; [b]Department of Materials Science, Montanuniversität Leoben, Leoben, Austria; [c]Microstructure and Properties of Materials (IMD-1), Forschungszentrum Jülich GmbH, Jülich, Germany

ABSTRACT

The effect of columnar grain boundaries (GBs) on the fracture toughness was investigated using micro-cantilever fracture testing in a hard coating featuring two distinct microstructures within a single sample: a columnar-grained top and an epitaxial bottom region. Bridge-notch fracture initiated more readily in the columnar-grained region, indicating reduced toughness. Furthermore, quantitative analysis of the load drops at bridge-failure confirmed a ~30% decrease in fracture toughness due to GBs: from 4.1 to 3.0 MPa $m^{1/2}$. These results reveal the detrimental role of GBs in fracture toughness and highlight the importance of microstructural design for improving the mechanical performance of hard coatings.

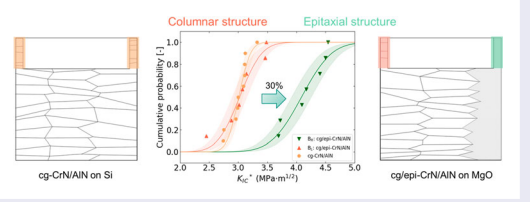

ARTICLE HISTORY
Received 13 July 2025

KEYWORDS
Grain boundary; fracture toughness; epitaxial structure; hard coating

1. Introduction

Hard coatings have been widely used for various industrial applications including cutting tools, protective layers for aerospace components, and wear-resistant surfaces for mechanical parts [1–3]. These coatings possess superior hardness, wear resistance, and thermal stability, thus effectively protect the metallic substrates and components [4–6]. However, one of their critical limitation is brittleness, more specifically, their limited fracture toughness. It is widely recognized that microstructural features such as grain boundaries (GBs) or point defects and their density can play a detrimental role in fracture toughness governing crack nucleation and propagation [7–9]. Typically, hard coatings, composed of oxides, nitrides, or carbides, are mostly fabricated using physical vapor deposition (PVD) method, however, PVD-grown coatings typically exhibit a columnar grain microstructure characterized by grain sizes below a few hundred nanometers [10, 11]. This results in a high density of GBs, which can further degrade fracture toughness [12–23]. For example, our recent study showed that the orientation of columnar grained microstructure with respect to the loading direction influences the crack propagation path thus fracture toughness as well [19].

Although GBs are widely recognized as the weak links in hard coatings and there have been many attempts to improve their mechanical properties via so-called GB engineering, the fundamental understanding of their quantitative impact on fracture toughness remains limited. Previous studies have explored the influence of GBs on the fracture toughness of hard coatings by comparing different hard coatings with different microstructures and GB density [24–26]. For instance, the fracture behavior of α-Al_2O_3 coatings was investigated through micro-cantilever bending tests, which reported slightly enhanced fracture toughness in single crystal coatings compared to polycrystalline ones [26]. Conversely, improvements in mechanical properties through GB engineering have also been reported in zirconia coatings [25]; the polycrystalline samples showed better crack resistance under nanoindentation compared to a single crystal.

CONTACT Subin Lee subin.lee@kit.edu Institute for Applied Materials, Karlsruhe Institute of Technology, Karlsruhe D-76131, Germany

Supplemental data for this article can be accessed online at https://doi.org/10.1080/21663831.2025.2560526.

One of the challenges to quantitatively measure the effect of GBs on fracture toughness is that various factors, besides GBs, influence the (apparent) fracture toughness of hard coatings, such as crystallographic texture, residual stress, off-stoichiometry, and elemental segregation. These intrinsic properties are strongly affected by the deposition process, where even small variations in the deposition parameters can significantly change the properties of the coatings [27, 28]. Consequently, synthesizing model systems that differ only in their content of columnar GBs while maintaining identical chemical and defect structures is extremely challenging, which has hindered quantitative insights into their effect on fracture toughness.

To address this gap, we conducted *in situ* scanning electron microscope (SEM) micro-cantilever fracture testing on CrN/AlN hard coatings. Two key approaches were used to investigate the influence of GBs on the fracture toughness of these nitride hard coatings. Firstly, a unique microstructure was introduced to the coating by controlling misfit strain: an epitaxial and single crystal in the bottom of the coating and the top part with a columnar-grained microstructure. Secondly, instead of a conventional through-thickness notch, a bridge notch with a thin side ligament was introduced to prepare micro-cantilevers. This approach minimizes FIB-induced artifacts and allows fracture toughness to be measured from small volumes, specifically from different regions of the coating with distinct microstructures. By combining these two approaches, we were successfully able to isolate the contribution of GBs to the fracture toughness from several other factors which could alter fracture toughness, and ultimately quantify the influence of the columnar GBs on the fracture toughness.

2. Materials and methods

CrN/AlN multilayered coatings, consisting of alternating layers of nominally 4 nm CrN and 2 nm of AlN, were deposited on MgO (100) and Si (100) substrates, respectively (detailed deposition processes can be found in our previous study [29]). Prior to deposition, the substrates were ultrasonically cleaned in acetone and ethanol, respectively. They were then mounted in an AJA ATC-1800 ultra-high vacuum deposition system, where they underwent thermal cleaning at 550°C for 30 minutes in a vacuum, followed by 5–10 minutes of Ar ion etching at 500°C. The Cr (diameter three-inch, purity 99.95%) and Al (diameter three-inch, purity 99.99%) targets were sputter-cleaned behind closed shutters for 5 minutes before film growth. The coatings were subsequently grown in pulsed DC mode (100 kHz pulse frequency, 1 μs pause). To ensure a dense morphology, 300 W was applied to the Cr target and 500 W to the Al target in a mixed N_2/Ar gas atmosphere (12 sccm/8 sccm flow rate ratio) at a total pressure of 0.2 Pa, combined with a −70 V DC bias applied to the substrates. The substrates were continuously rotated at approximately 0.5 Hz during deposition. The multilayered structure was achieved through computer-controlled opening and closing of mechanical shutters at specific intervals. The total thickness of the CrN/AlN multilayered coatings was 1.9 μm.

The microstructure of the coating was characterized firstly using SEM (Merlin Gemini II, Zeiss), focused ion beam (FIB, Crossbeam 550L, Zeiss) and transmission electron microscopy (TEM, Titan Themis 300, Thermo Fisher Scientific) to study their grain structure, orientation relationship and chemical distribution. Subsequently, micro-cantilevers with square cross-sections were fabricated using FIB milling with 30 kV Ga^+ ions and ion currents of 15 nA, 3 nA, 700 pA, and 50 pA for stepwise milling. The dimensions of the micro-cantilevers were kept consistent with an L:W:B ratio of 5:1:1, where L is the distance to the loading point from a notch, W is the thickness, and B is the width of the micro-cantilever as shown in Figure 1. As the coating thickness, W, is pre-determined to 1.9 μm by the coating synthesis, their width was adjusted to have a square cross-section.

A bridge notch rather than a through-thickness notch was employed. As demonstrated in our previous studies [29, 30], with a bridge-notch, fracture typically initiates from the bridge failure, where an atomically sharp crack is generated via crack arrest, thereby reducing the scatter in the measured fracture toughness values. In the present work, the bridge notch geometry was specifically utilized to enable the determination of apparent fracture toughness in local regions of the coatings. For this purpose, a notch with a depth, a, ranging from 20–30% of the thickness W was introduced using a 20 pA and 30 kV ion beam. The width of the notch, b, was chosen to yield a b/B ratio of 0.92 to maximize stress localization and promote bridge-failure with subsequent crack arrest. Finally, each of the ligaments (or bridge) was a width of less than 100 nm.

The cantilevers were prepared in two geometries with different orientations relative to the coating growth direction, as shown in Figure 1. In one case, the loading direction was parallel to the growth direction (Figure 1(a,c)), whereas in the other case it was perpendicular (Figure 1(b,d)).

Micro-fracture experiments were performed *in situ* using a nanoindenter (Hysitron PI-89, Bruker) equipped with a 10 μm diamond wedge tip (Synton-MDP AG) in an SEM (Merlin Gemini II, Zeiss). All tests were conducted in a displacement-controlled mode at 5 nm/s

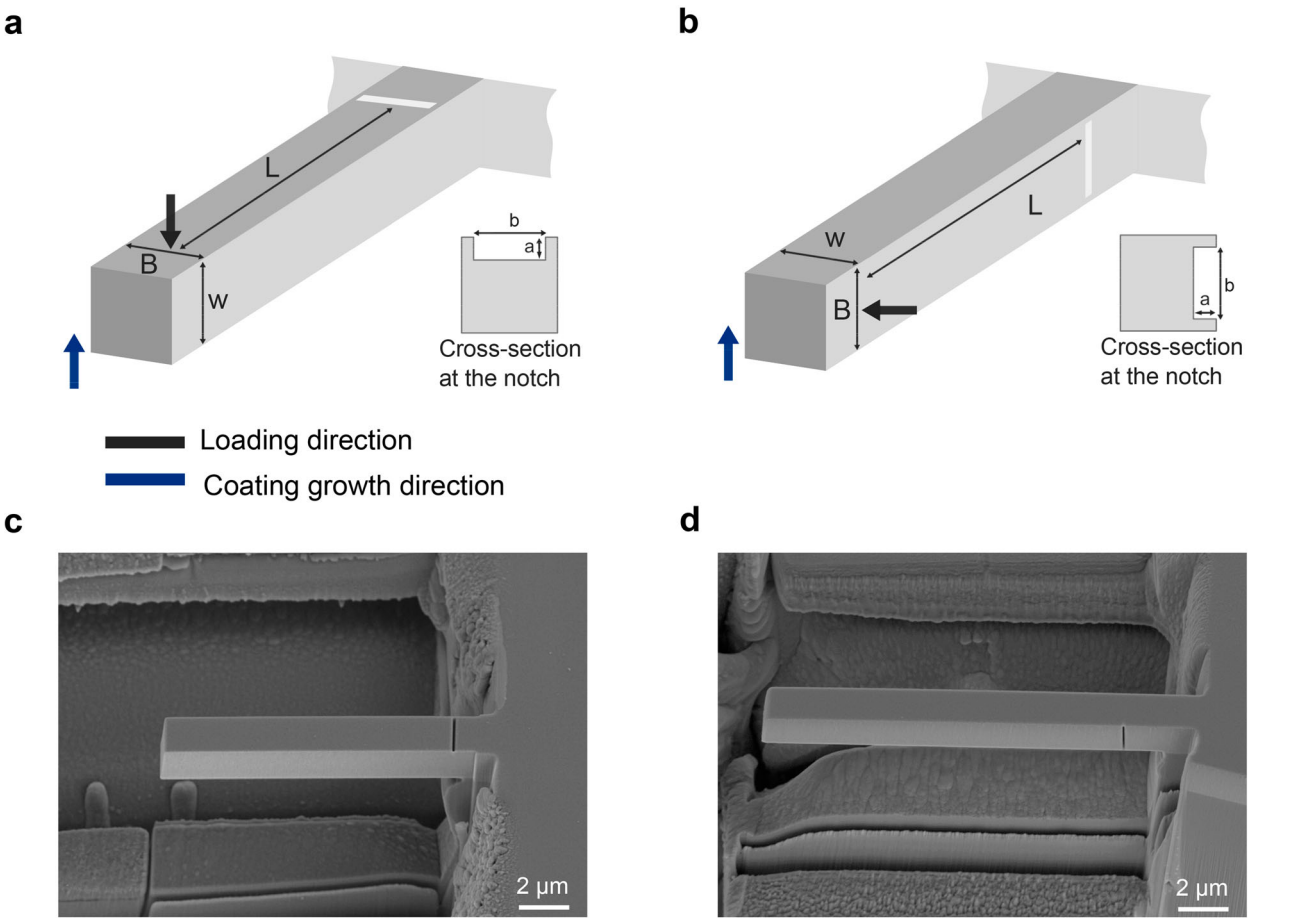

Figure 1. (a, b) Schematics of the cantilever geometries and their orientation relative to the loading direction. (c, d) Representative SEM images of each geometry. In (c), the loading direction is parallel to the coating growth direction (i.e. along the columnar grain microstructure), whereas in (d) it is perpendicular to the growth direction.

using a transducer with a maximum load of 10 mN and a noise floor of 0.4 μN. The fracture toughness, K_{IC}, is evaluated at the point of final failure of the specimens. At this point, the two bridges had already failed, and the final fracture occurred at the arrested natural crack [29, 30]. This protocol follows Matoy's pioneering work, introduced in [31],

$$K_{IC} = \frac{F_C L}{BW^{\frac{3}{2}}} f_{Matoy}\left(\frac{a}{W}\right) \tag{1}$$

where, F_C is the load at final fracture, and $f_{Matoy}\left(\frac{a}{W}\right)$ is a geometry shape factor defined by:

$$f_{Matoy}\left(\frac{a}{W}\right) = 1.46 + 24.36(a/W) - 47.21(a/W)^2 + 75.18(a/W)^3 \tag{2}$$

The fracture toughness $K_{Ic}{}^*$represents the fracture toughness at bridge-failure. It can be calculated using the geometry correction factor f_{corr} [29, 31, 32]:

$$K_{IC}{}^* = \frac{F_B L}{BW^{\frac{3}{2}}} f_{Matoy}\left(\frac{a}{W}\right) / f_{corr} \tag{3}$$

where, F_B represents the load at bridge-failure. Note that two additional fracture toughness values can be obtained per micro-cantilever from each bridge failure, for those cases where a clear load drop, bridge failure and crack arrest are observed *in situ*.

3. Results and interpretation

A CrN/AlN multilayer coating with individual layer thicknesses of 4 nm (CrN) and 2 nm (AlN) was deposited on both MgO and Si substrates under the same conditions. Despite the identical deposition process, the coatings exhibited distinct microstructures. Firstly, the coating on a MgO (100) substrate had two distinct microstructures within the film, as schematically depicted in Figure 2(a): a roughly 500 nm-thick epitaxial structure is formed at the bottom (see Figure 2(b)

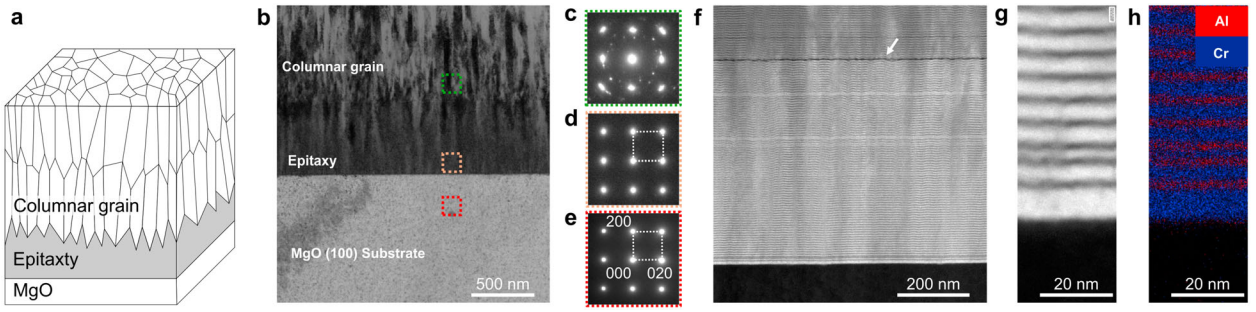

Figure 2. Microstructure investigation of cg/epi-coating. (a) Schematic drawing of the cg/epi-coating with an epitaxial layer between the columnar-grained microstructure and the MgO (100) substrate. (b) TEM image of the cross-section of the cg/epi-coating. Selected area diffraction patterns from (c) the columnar-grained microstructure, (d) the epitaxial structure, (e) and the MgO (100) substrate. (f) HAADF-STEM image of the epitaxial part and the interface with MgO substrate. (g) HAADF-STEM image at higher magnification on the epitaxial part showing CrN and AlN multi-layered structure and (h) its corresponding EDS maps. The target thickness of CrN and AlN layers were 4 and 2 nm, respectively.

and (d)), which is followed by a columnar-grained microstructure (compare Figure 2(c) and (d)). The column diameter in the upper part of this coating is about 70 nm. In contrast, the coating deposited on a Si (100) substrate exhibited only a columnar-grained structure with comparable columnar diameter (approximately 100 nm) of the one on a MgO substrate. Hereafter, the coating on MgO will be referred to as columnar grain/epitaxial (cg/epi) coating, while the one on Si will be referred as columnar grain (cg) coating.

TEM selected area electron diffraction patterns from each part of the cg/epi-coating (Figure 2(c)–(e)) showed the (100) cube-on-cube orientation relationship between the MgO substrate and the epitaxial part in Figure 2(d), which is largely maintained in the upper part as well. Scanning TEM (STEM) high-angle annular dark-field (HAADF) imaging and energy dispersive spectroscopy (EDS) mapping reveal the layered microstructure of the coating (Figure 2(f)–(h)). Faulted layers as indicated by an arrow in Figure 2(f), show darker contrast compared to other layers suggesting lower atomic density. Since it is located near the point where the transition from the epitaxial to columnar microstructure occurred, it is speculated that due to the accumulated strain energy from the epitaxial growth, the faulted layer was formed and altered the microstructure of the layers deposited afterwards. Further comparisons of the columnar grain structures in the cg- and cg/epi-coatings, including HAADF-STEM imaging, electron diffraction, and STEM-EDS composition analysis, are provided in Figure S2 of the Supplementary materials.

The influence of the epitaxial structure on the fracture toughness of the coating was investigated firstly by comparing the fracture toughness of cg/epi and cg-coating. A representative SEM image of the experimental setup, a cantilever and a wedge tip, is shown in Figure 3(a). In both samples, the load-displacement curves, 8 curves from cg/epi-coatings (Figure 3(b)) and 11 curves from cg-coatings [29], exhibited linear elastic behavior until bridge failure (points B1 and B2) with subsequent crack arrest. From each of the three load drops (B1, B2, and C), fracture toughness values can be determined. For the first two drops corresponding to bridge failure, the apparent fracture toughness K_{IC}* was obtained using Equation 3, while for the final fracture event (C), K_{IC} was calculated using Equation 1. Representative load-displacement curves are shown in Supplementary Figure S3.

Cumulative probability distribution of the fracture toughness, K_{IC} calculated using the final failure (F_C), in Figure 3(c), clearly demonstrates that K_{IC} of cg/epi-coating is higher than that of cg-coating. The mean K_{IC} value is 3.1 ± 0.1 MPa $m^{1/2}$ for cg/epi-coating while 2.7 ± 0.1 MPa $m^{1/2}$ [29] for cg-coating with the standard deviation representing the scatter band. The shaded region in Figure 3(c) represents the normal distribution fit with its 95% confidence band, and the detailed data used for the calculation are provided in Supplementary Table S1. Although the epitaxial part was located at the bottom of the coating and comprised only a quarter of the total thickness, it notably enhanced the fracture toughness by nearly 15%.

A comparison of the fracture surfaces reveals a flat morphology in the epitaxial region adjacent to the MgO substrate (Figure 3(d,e)), whereas the cg region and the upper part of the cg/epi-coating show rough surfaces, suggesting predominantly intergranular fracture. This reduction in roughness in the epitaxial region indicates a change in crack path once the crack enters the bottom layer. Consequently, even though the notch was positioned in the cg region, the underlying epitaxial layer contributes to the overall fracture resistance of the cg/epi-coating, leading to the slightly higher measured K_{IC} in

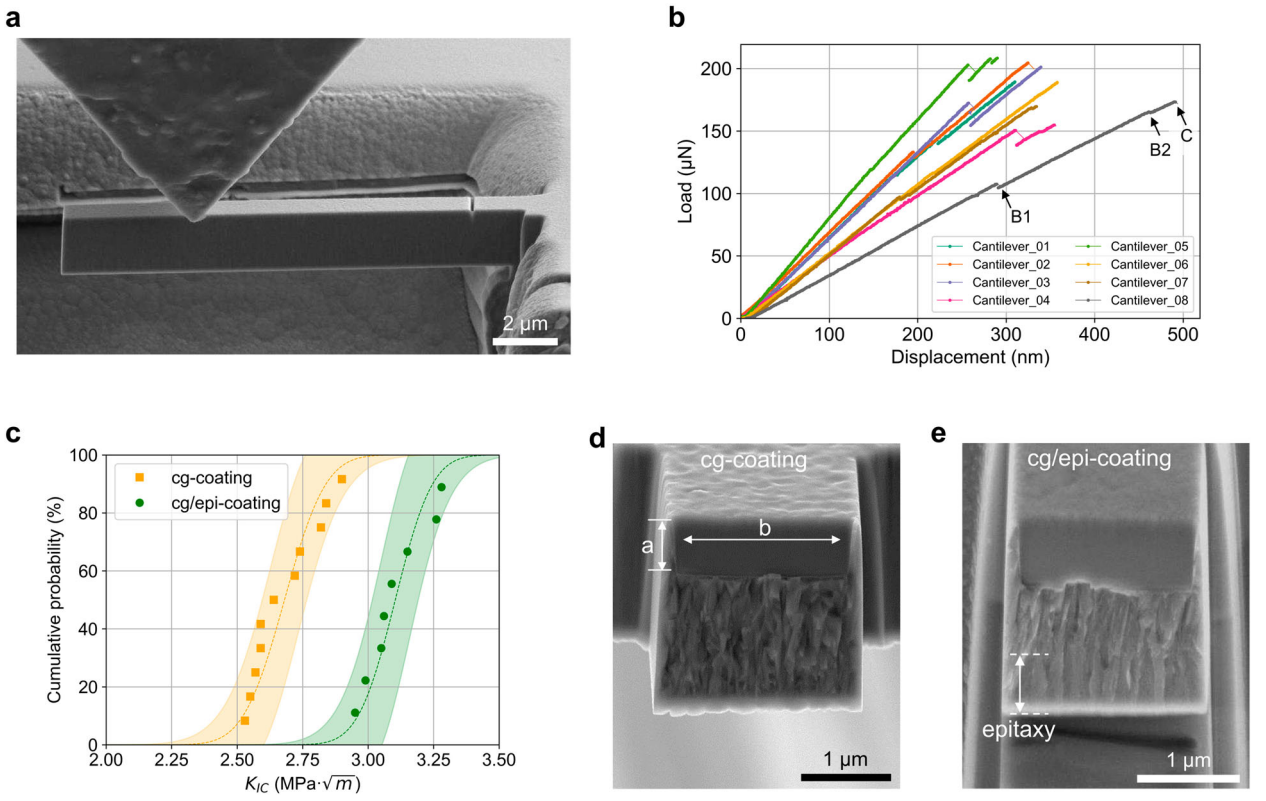

Figure 3. (a) Free-standing micro-cantilever of the cg/epi-coating. (b) Load-displacement curves from 8 micro-cantilever bending tests of the cg/epi-coating. The failure of the material bridges, B1 and B2, and the final fracture, C, are indicated on one representative curve. (c) Cumulative distribution of the fracture toughness, K_{IC}, for the cg/epi-coating and cg-coatings at point C. The cg/epi-coating with epitaxial structures exhibited higher fracture toughness. The shaded band indicates 95% confidence intervals of the normal distribution fitting. (d) SEM image of the fracture surface of the cg-coating and (e) the cg/epi-coating. Intergranular fracture is visible in the cg-coating and the top part of the cg/epi-coating.

Figure 3. To further quantify the contributions of the columnar and epitaxial regions, we performed dedicated bridge-notch experiments, as described in the following section.

To determine the apparent fracture toughness of the columnar-grained and the epitaxial microstructure, we employed bridge notches in 90-degree rotated micro-cantilevers (compare the growth directions in Figure 4(a)). This approach allows for positioning each material bridge in either of the two microstructures in epi/cg-coating, and measure the apparent fracture toughness from the local region of the coating.

We first analyzed the bridge-failure sequence, i.e. the temporal occurrence of failure of each bridge. By correlating the *in situ* SEM video with the load drops in the load–displacement curves, we could determine which bridge (left or right) fractured first. For example, Figure 4(b,c) shows the failure of the left bridge while the other still remained intact. The statistics of the failure sequence (Figure 4(d)) provide a clear indication of the weaker bridge: in the case of cg/epi-coatings, the columnar-grained microstructure (left bridge) failed first, whereas a uniform distribution was found for the cg-coating. Additional *in situ* SEM snapshots showing the failure sequences of both coatings can be found in Supplementary Figure S4. The differences in failure sequence in the cg/epi sample clearly demonstrate the contrasting fracture behavior of the epitaxial and columnar microstructures, and qualitatively indicates that the columnar grain boundaries are indeed the weakest link in hard coatings, exhibiting lower fracture toughness compared to the epitaxial microstructure.

Besides the failure sequence, we also used the load drops (B1 and B2 in Figure 3(b)) caused by bridge-failure to calculate the local apparent fracture toughness $K_{IC}*$ from bridge-failure using Equation (3). In brittle ceramics, extrinsic toughening is often considered the primary mechanism for enhancing toughness, as discussed by Lawn [33]. For example, the fracture toughness of traditional polycrystalline SiC is typically 2.5–4 MPa $m^{1/2}$ [34], but can increase to ~9.1 MPa $m^{1/2}$ when intergranular fracture dominates [35, 36]. One might expect significantly higher fracture toughness in the columnar microstructure than in the epitaxial layer. However, the

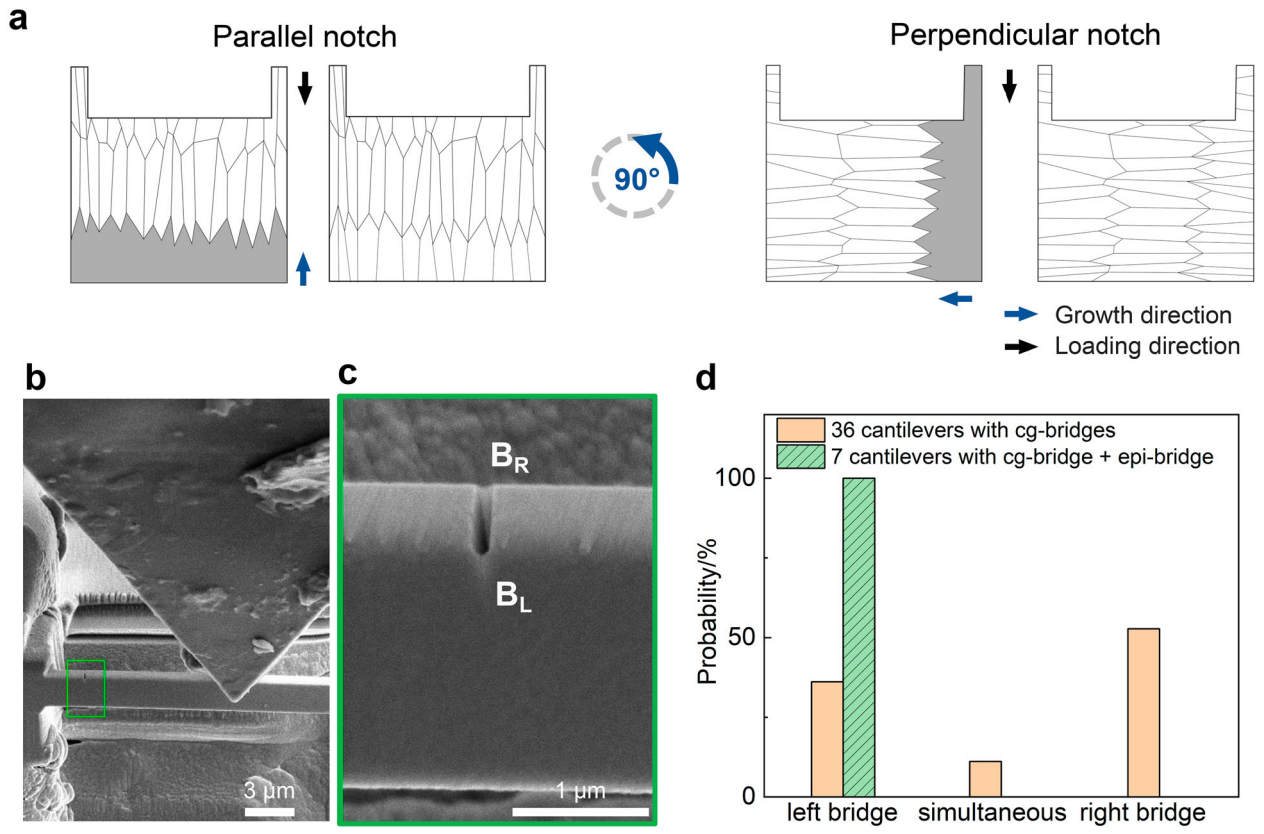

Figure 4. (a) The schematics showing cross-sections of micro-cantilevers with bridge notches. Material bridges were positioned within each microstructure, i.e. the columnar grain and epitaxial microstructure, by rotating the coating 90 degrees. (b) Screen shot from test video, and (c) its enlarged view, where the bridge on the observed tip side is defined as the left bridge (B_L) and the opposite as the right bridge (B_R) (d) Statistics of bridge-failure sequence. The orange bars represent 36 micro-cantilevers only with cg-bridges, and the green bar shows 7 micro-cantilevers from the cg/epi-coating with a cg-bridge on the left and an epi-bridge on the right side. The failure sequence is random when the microstructure of both bridges is similar, while in the cg/epi-coating, the bridge with epitaxial microstructure was always broken after the columnar one.

epitaxial bridge showed a fracture toughness (denoted K_{IC}*-B_R) of 4.1 ± 0.4 MPa $m^{1/2}$, which is higher compared to that of the columnar-grained bridge (K_{IC}*-B_L), which is 3.0 ± 0.3 MPa $m^{1/2}$ (see Figure 5(a)). The critical loads and sample dimensions for the determination of K_{IC}* are provided in the Supplementary Table S2. Although the two samples were deposited on different substrates, the latter value is similar to experiments on a cg-coating in similar geometry i.e. with crack propagation perpendicular to the growth direction (see the orange markers in Figure 5(a), 3.0 ± 0.2 MPa $m^{1/2}$). This is another indication that the fracture toughness of such brittle hard coatings is dominated by microstructure, more specifically, GB structure, as the microstructure in the left bridge (B_L) is comparable to the one in the cg-coating.

In addition to these quantitative measurements, the fracture surfaces also revealed clear differences between the epitaxial and the columnar microstructures. While the fracture surface is rough across the cross-section in the case of cg-coating (Figure 5(b)), indicating intergranular fracture, the right side of the fracture surface of the cg/epi-coating was smooth, characteristic of intragranular fracture in the epitaxial microstructure (Figure 5(c)). Further images of the fracture surfaces are shown in Figure S5 in the Supplementary materials.

4. Discussion

In the first dataset, where the crack propagates along the growth direction (Figure 3), the FIB notches of both samples were located within the columnar-grain region, regardless of their overall microstructure. The results show a higher overall fracture toughness for the cg/epi-coating, suggesting that epitaxial growth enhances toughness. However, the contribution of the epitaxial region cannot be quantitatively separated from this dataset.

In contrast, for samples rotated by 90°, such a separation becomes possible due to the thin material bridges. The right bridge (B_R) of the cg/epi-coating is epitaxial and free of columnar GBs, thus the obtained

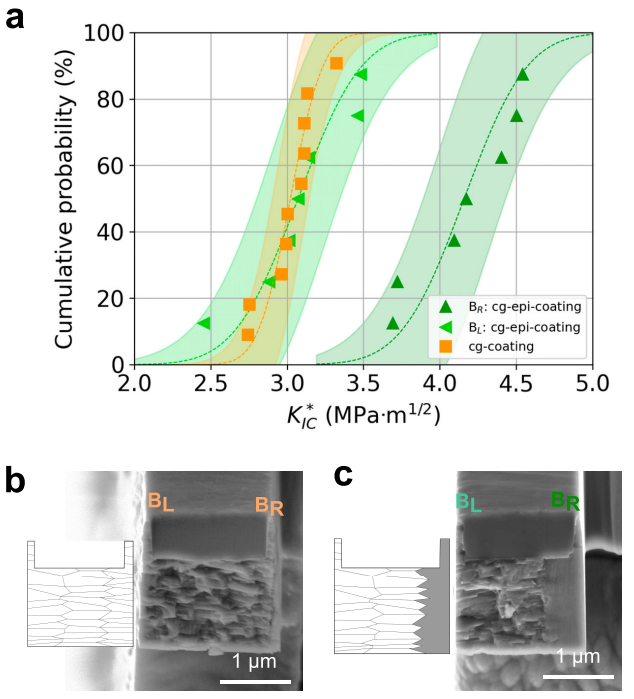

Figure 5. Comparison of the apparent fracture toughness from bridge-failures of two microstructures, and their fracture surface. (a) The cumulative distribution functions of the fracture toughness $K_{IC}*$ derived from bridge-failure of the cg-coating, and the cg/epi-coating with crack growth perpendicular to the film growth direction. The bands represent 95% confidence intervals. (b) SEM images of the fracture surface of the cg-coating and (c) the cg/epi coatings.

toughness values represent the fracture toughness of the epitaxial-GB free coating (Figure 5). The left bridge (B_L), however, exhibits columnar grain boundaries similar to those in cg-coating. Consequently, the fracture toughness values of the left bridge for both samples are in same range because of the similar microstructure. This configuration enables a direct separation and quantitative assessment of the detrimental role of columnar grain boundaries in reducing the fracture toughness of hard coatings.

The role of grain boundaries in fracture toughness has long been debated in the community. While some studies suggest that grain boundaries are detrimental, others report that they can enhance toughness by activating toughening mechanisms such as crack deflection or branching. Our results show that in the case of catastrophic failure of a brittle material, grain boundaries act as weak links compared to epitaxial regions or single-crystal-like grain interiors, where the higher atomic density requires greater energy for crack propagation. In particular, random high-angle grain boundaries, which are the most common type in engineering materials, represent less densely packed structures and therefore provide preferential crack paths that reduce toughness.

In polycrystalline materials with relatively large grains, however, grain boundaries may contribute to toughening through the aforementioned mechanisms if their orientation impedes straight crack propagation. R. Daniel et al. [18], for example, demonstrated crack deflection at grain-boundary junctions as a toughening mechanism. Similarly, our recent work on CrN and AlN coatings showed improved fracture toughness when multiple crack kinking was activated [19]. In that case, the fracture toughness increased from 2.7 ± 0.1 MPa m$^{1/2}$ when the crack propagated parallel to the columnar texture to 3.0 ± 0.2 MPa m$^{1/2}$ in the perpendicular orientation. In summary, individual grain boundaries are weaker than single-crystal regions under crack propagation, but their collective distribution may either decrease or enhance fracture toughness depending on geometry. In typical PVD-grown hard coatings, where columnar grain boundaries dominate, they act predominantly as easy crack paths, which limits its fracture toughness and highlights the potential of grain-boundary engineering.

Beyond the structural role of grain boundaries, chemical segregation could also influence the mechanical response. Since no post-deposition heat treatment was applied in our experiment, significant segregation is not expected. Nevertheless, to exclude this possibility, we have performed STEM-EDS, which didn't show noticeable GB segregation (e.g. from Ga). Therefore, the significantly higher fracture toughness in the epitaxial part compared to the columnar grain part is expected to originate from its inherent properties of the single crystal and generally weak GBs at the columnar grain structure, but not from grain boundary weakening caused by segregation.

A noteworthy aspect is the role of residual stress. Residual stress is inevitably introduced during deposition and may differ between the cg- and cg/epi-coatings due to the different substrates. However, in the present microcantilever geometry (single beam, $\sim 2\ \mu$m thick), most of the residual stress was released during fabrication. This was confirmed by the observation that cg-coatings remained nearly straight after being cut from the substrate, while cg/epi-coatings showed a slight downward bending, indicating elastic relaxation of residual stress (Supplementary Figure S6). Therefore, in the present study, the influence of residual stress on the measured fracture toughness is considered negligible compared to the effect of microstructure.

Finally, other crystal defects inside a grain, for example, point defects or voids, could also influence the fracture toughness. Since the coating was deposited in

a single deposition process and no additional heat treatment was conducted, we don't expect substantial fluctuation in the defect density within different positions of the coating.

5. Conclusion

In conclusion, columnar grain boundaries clearly act as the weakest link in the fracture of hard coatings. This study provides a quantitative assessment of the decrease in their resistance to crack growth with bridge notch micro-cantilevers. The low grain boundary toughness was demonstrated both qualitatively through the failure sequence of the sample bridges, and quantitatively through fracture toughness measurements at bridge-failure, using samples with two distinct microstructures in one coating: columnar grains and an epitaxial seed layer. The apparent fracture toughness measured from the bridges composed solely of the epitaxial microstructure was found to be around 30% higher compared to that of the columnar grains (compare 4.1 ± 0.4 MPa $m^{1/2}$ and 3.0 ± 0.3 MPa $m^{1/2}$).

Acknowledgements

This research was funded within the framework of the DACH program by the national funding agencies: Austrian Science Fund (FWF) [I4720] and German Research Foundation (DFG) [436506789]. Support from the Helmholtz Program Materials Systems Engineering and from the Robert-Bosch-Foundation is gratefully acknowledged. The authors thank M. T. Becker for the film deposition, the Karlsruhe Nano Micro Facility (KNMFi) for support and access to TEM facilities and R. Pippan from the Austrian Academy of Sciences for helpful discussions.

Disclosure statement

No potential conflict of interest was reported by the author(s).

Funding

This work was supported by Austrian Science Fund: [Grant Number I4720]; Deutsche Forschungsgemeinschaft: [Grant Number 436506789].

Date availability

Data will be made available on request.

References

[1] Schalk N, Tkadletz M, Mitterer C. Hard coatings for cutting applications: physical vs. chemical vapor deposition and future challenges for the coatings community. Surf Coat Technol. 2022;429:127949.
[2] Mayrhofer PH, Mitterer C, Hultman L, et al. Microstructural design of hard coatings. Prog Mater Sci. 2006;51(8):1032–1114.
[3] Tkadletz M, Schalk N, Daniel R, et al. Advanced characterization methods for wear resistant hard coatings: a review on recent progress. Surf Coat Technol. 2016;285:31–46.
[4] Sidky P, Hocking M. Review of inorganic coatings and coating processes for reducing wear and corrosion. Br Corros J. 1999;34(3):171–183.
[5] Miller P, Holladay J. Friction and wear properties of titanium. Wear. 1958;2(2):133–140.
[6] Mayrhofer PH, Rachbauer R, Holec D, et al. Protective transition metal nitride coatings. In: Hashmi S, Batalha GF, Tyne CJV, editors. Comprehensive materials proceedings Vol. 4. Amsterdam: Elsevier; 2014. p. 355–388. doi:10.1016/B978-0-08-096532-1.00423-4
[7] Faber KT, Evans AG. Crack deflection processes—I. Theory. Acta Metall. 1983;31(4):565–576.
[8] Hahn GT. The influence of microstructure on brittle fracture toughness. Metall Trans A. 1984;15(6):947–959.
[9] Best JP, Zechner J, Shorubalko I, et al. A comparison of three different notching ions for small-scale fracture toughness measurement. Scr Mater. 2016;112:71–74.
[10] Stewart JA, Spearot DE. Phase-field simulations of microstructure evolution during physical vapor deposition of single-phase thin films. Comput Mater Sci. 2017;131:170–177.
[11] Thornton JA. High rate thick film growth. Annu Rev Mater Sci. 1977;7(1):239–260.
[12] Völker B, Stelzer B, Mráz S, et al. On the fracture behavior of Cr2AlC coatings. Mater Des. 2021;206:109757.
[13] Riedl A, Daniel R, Stefenelli M, et al. A novel approach for determining fracture toughness of hard coatings on the micrometer scale. Scr Mater. 2012;67(7-8):708–711.
[14] Gopalan H, Marshal A, Hans M, et al. On the interplay between microstructure, residual stress and fracture toughness of (Hf-Nb-Ta-Zr) C multi-metal carbide hard coatings. Mater Des. 2022;224:111323.
[15] Schoof MR, Karimi Aghda S, Kusche CF, et al. The influence of microstructural orientation on fracture toughness in (V, Al)N and (V, Al)(O, N) coatings as measured by microcantilever bending. J Mater Res. 2023;38(16):3950–3965.
[16] Liu L, Ruan Q, Wu Z, et al. Hard and tough CrN coatings strengthened by high-density distorted coherent grain boundaries. J Alloy Compd. 2022;894:162139.
[17] Meindlhumer M, Ziegelwanger T, Zalesak J, et al. Precipitation-based grain boundary design alters Inter- to Trans-granular Fracture in AlCrN Thin Films. Acta Mater. 2022;237:118156.
[18] Daniel R, Meindlhumer M, Baumegger W, et al. Grain boundary design of thin films: using tilted brittle interfaces for multiple crack deflection toughening. Acta Mater. 2017;122:130–137.
[19] Zhang Y, Bartosik M, Brinckmann S, et al. Toughening nitride hard coatings by deflecting cracks along grain boundaries. Mater Sci Eng A. 2025;935:148392.
[20] Best JP, Zechner J, Wheeler JM, et al. Small-scale fracture toughness of ceramic thin films: the effects of specimen geometry, ion beam notching and high temperature on chromium nitride toughness evaluation. Philos Mag. 2016;96(32-34):3552–3569.

[21] Glechner T, Lang S, Hahn R, et al. Correlation between fracture characteristics and valence electron concentration of sputtered Hf-CN based thin films. Surf Coat Technol. 2020;399:126212.
[22] Mishra AK, Gopalan H, Hans M, et al. Strategies for damage tolerance enhancement in metal/ceramic thin films: Lessons learned from Ti/TiN. Acta Mater. 2022;228:117777.
[23] Gibson JS-L, Rezaei S, Rueß H, et al. From quantum to continuum mechanics: studying the fracture toughness of transition metal nitrides and oxynitrides. Mater Res Lett. 2018;6(2):142–151.
[24] Mathews NG, Lambai A, Mohanty G, et al. Effect of stiff substrates on enhancing the fracture resistance of Barium Titanate thin films. Mater Des. 2023;235:112440.
[25] Henry R, Le Roux N, Zacharie-Aubrun I, et al. Indentation cracking in mono and polycrystalline cubic zirconia: methodology of an apparent fracture toughness evaluation. Mater Sci Eng A. 2022;860:144261.
[26] Konstantiniuk F, Tkadletz M, Kainz C, et al. Mechanical properties of single and polycrystalline α-Al2O3 coatings grown by chemical vapor deposition. Surf Coat Technol. 2021;410:126959.
[27] Baptista A, Silva F, Porteiro J, et al. Sputtering physical vapour deposition (PVD) coatings: a critical review on process improvement and market trend demands. Coatings. 2018;8(11):402.
[28] Mayrhofer PH, Mitterer C. Structure/property relations in PVD hard coatings. In: Pandalai SG, editors. Recent research developments in vacuum science & technology. Vol. 4. Trivandrum: Transworld research network; 2003. p. 71–97.
[29] Zhang Y, Bartosik M, Brinckmann S, et al. Direct observation of crack arrest after bridge notch failure: a strategy to increase statistics and reduce FIB-artifacts in microcantilever testing. Mater Des. 2023;233:112188.
[30] Okotete E, Muslija A, Hohmann JK, et al. Enhanced crack stability in micro scale fracture testing via optimized bridge notches. Mater Sci Eng A. 2025;939:148479.
[31] Matoy K, Schönherr H, Detzel T, et al. A comparative micro-cantilever study of the mechanical behavior of silicon based passivation films. Thin Solid Films. 2009;518(1):247–256.
[32] Brinckmann S, Matoy K, Kirchlechner C, et al. On the influence of microcantilever pre-crack geometries on the apparent fracture toughness of brittle materials. Acta Mater. 2017 2017-09-01;136:281–287.
[33] Lawn B. Fracture of Brittle Solids. second ed Cambridge: Cambridge University Press; 1993.
[34] Delage J, Saiz E, Al Nasiri N. Fracture behaviour of SiC/SiC ceramic matrix composite at room temperature. J Eur Ceram Soc. 2022;42(7):3156–3167.
[35] Ritchie RO. The conflicts between strength and toughness. Nat Mater. 2011;10(11):817–822.
[36] Gilbert C, Cao J, De Jonghe L, et al. Crack-growth resistance-curve behavior in silicon carbide: small versus long cracks. J Am Ceram Soc. 1997;80(9):2253–2261.